Observations and Modeling of the Sea Breeze with the Return Current

A. B. C. TIJM, A. A. M. HOLTSLAG,* AND A. J. VAN DELDEN

Institute for Marine and Atmospheric Research, Utrecht University, Utrecht, the Netherlands

(Manuscript received 19 February 1997, in final form 2 April 1998)

ABSTRACT

Data from a wind profiler are used to investigate the vertical structure of the sea breeze with the accompanying return current at the North Sea coast in the Netherlands for three sea-breeze cases. In one of the cases, with a very weak and constant background flow, the return current mass flux approximately compensates for the sea-breeze mass flux. To study the sea breeze with the accompanying return current, a simple two-dimensional mesoscale model is constructed. It is found that the sea breeze as well as the return current of the three cases in this study are simulated well by the model. In the case mentioned above, the model indicates an overcompensation of the sea breeze by the return current. It is found that the latter is a function of the initial vertical temperature profile and the depth of the boundary layer, and that it can be as much as 30%. The overcompensation is balanced by a mass flow (in the sea-breeze direction) at a larger height (''return–return current''). As such, a three-layer structure for the sea breeze becomes evident.

1. Introduction

Land and sea breezes are still the subject of many articles found in the meteorological literature. The different studies can be put into different categories, according to the methods used. The observational studies always depend strongly on the available measuring equipment. Due to the lack of good instruments, the first sea-breeze studies, performed in the last part of the nineteenth century, consisted mainly of observing how far the sea breeze reached inland (Simpson 1994). More recently, sea breezes have been observed with the help of aircraft (Kraus et al. 1990; Finkele et al. 1995) and remote sensing techniques such as pulsed Doppler lidar (Banta et al. 1993; Banta 1995) and dual Doppler radar (Kingsmill 1995; Laird et al. 1995).

Theoretical studies can be split into the analytical and the numerical studies. Examples of the analytical sort are the studies performed by Schmidt (1947), Rotunno (1983), and Dalu and Pielke (1989). Sea breezes are also studied with the help of 2D and 3D numerical models. The first numerical study was performed by Estoque (1962), who used a 2D model to study the effects of the temperature difference and the large-scale wind on the development of the sea breeze. One of the first 3D studies was performed by Pielke (1974), whereas recently Bechtold et al. (1991) and Arritt (1993) use 2D models to study sea breezes under a wide range of conditions (i.e., large-scale winds, stability). The most recent studies involved nonhydrostatic models with which the turbulent properties of sea breezes (Koo and Reible 1995a,b) and Kelvin–Helmholtz instabilities in gravity currents (Xu et al. 1996) were studied.

All these numerous studies have helped to provide insight into the origin and development of the sea breeze. Nevertheless, there are still a few aspects of the sea breeze that have not been studied very extensively, probably due to the lack of good measuring equipment. A few of these aspects have been enumerated in the review of *Coastal Meteorology* (National Research Council 1992) with one aspect being the return current. By the return current we mean the compensatory flow for the thermally driven sea breeze.

Frizzola and Fisher (1963) found that the return current is difficult to detect, particularly in the presence of a large-scale wind. However, Atkinson (1981) shows a table with 17 observational studies that indicate that the return current does exist. In a recent study, Banta et al. (1993) found no observational evidence of a return current for Monterey Bay. In a more recent study, Banta (1995) found some evidence of a return current, although it did not fully compensate the sea breeze, as should be expected from continuity in a calm environment. More convincing evidence of a return current was published in a study performed by Finkele et al. (1995), who used cross sections measured with an airplane to derive a complete sea-breeze circulation cell.

* Additional affiliation: KNMI, Royal Netherlands Meteorological Institute, De Bilt, the Netherlands.

Corresponding author address: Dr. A. B. C. Tijm, KNMI, Postbus 201, 3730 AE De Bilt, the Netherlands.
E-mail: tijm@knmi.nl

In this paper observations and simulations of three sea-breeze cases in the Netherlands with relatively pronounced return currents will be described and analyzed. In one of the cases, the air mass transported by the return current approximately equals and possibly exceeds the air mass transported by the sea breeze. We will give an explanation of these findings in section 6. Section 2 provides a description of the measuring equipment and of the area where the measurements are made. In section 3 we will describe the three sea-breeze cases with emphasis on the measurements made with a wind profiler located 45 km inland. In section 4 we will describe a numerical model, which is used to simulate the sea breeze and its return current. Section 5 discusses the results of these simulations.

2. Observation area

The coastline of the Netherlands is nearly straight (see Fig. 1) and orography is almost absent. In the first 50 km the most significant orography is an area with sand dunes in the first few kilometers from the coast. These dunes have maximum heights of about 10–20 m above sea level in the area of interest. Farther north the highest point lies at 57 m, whereas hills with a height exceeding 100 m lie more than 80 km inland. Apart from the sand dunes, the area behind the coast consists mainly of flat grassland with scattered villages and towns. Therefore the sea breeze can be studied almost in a pure form, undisturbed by orography and inhomogeneous vegetation cover.

The Netherlands has a dense network of synoptic stations where routine measurements are made with a time interval of 1 h. This means that a large amount of surface data is always available without the need for a special field campaign to obtain this data. Profiles of the wind and temperature are also measured on a routine basis at De Bilt (station 260, 50 km inland, see Fig. 1), where a radiosonde is launched every 6 h.

At Cabauw (station 348, 45 km inland, see Fig. 1) a 200-m meteorological tower is present at which vertical profiles of the wind, moisture, and temperature are measured on a routine basis. In July 1994, a 1290-MHz vertical wind profiler together with a Radio-Acoustic Sounding System was installed at Cabauw by the Royal Netherlands Meteorological Institute (KNMI). With these instruments, hourly averaged vertical profiles of the wind and temperature are measured up to a height of a few kilometers, depending on the atmospheric conditions. For an overview of the reliability and quality of the measurements we refer to Engelbart et al. (1996).

All these observations provide a good picture of the behavior of the sea breeze, especially near the surface. On days with a very weak background flow, when sea breezes travel up to 50 or 100 km inland, the vertical structure of the sea breeze arriving at Cabauw is measured in detail.

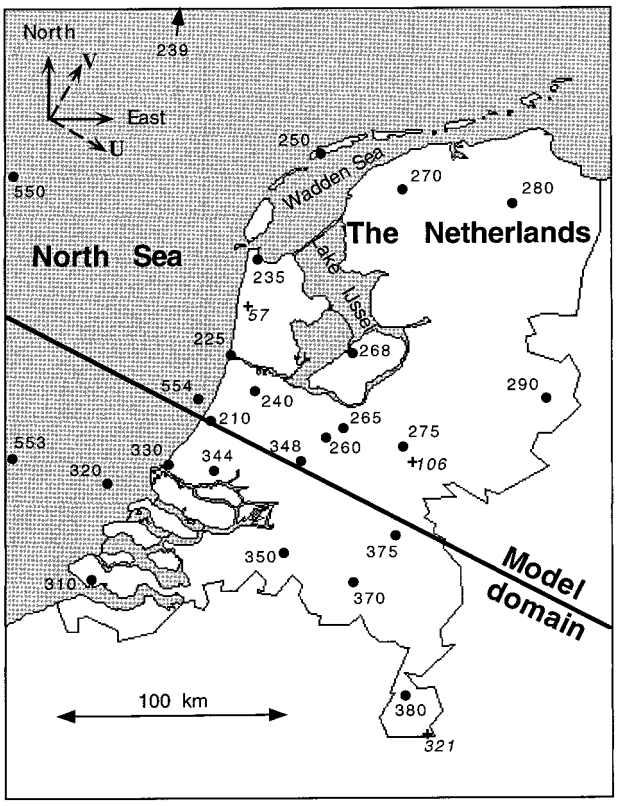

FIG. 1. The Netherlands with the observation stations, the 2D model domain, the orientation of the *U* and *V* components, and some surface elevations.

3. Observations

On 27 April 1996, an extremely well-developed sea-breeze front occurs that travels far inland. The synoptic situation is dominated by two areas of high pressure, one over Eastern Europe, the second over the Atlantic Ocean, west of Ireland. This situation results in a very flat pressure distribution over the Netherlands. In the resulting weak flow and under clear skies ahead of a cold front a sea breeze develops with the sea-breeze front well detectable from the surface observations. The sea surface temperature is about 7°C. The early morning radiosounding of this case (0600 UTC, see Fig. 2) shows a stable temperature profile, a nighttime inversion near the surface, and two layers of enhanced stability, between 1100 and 1400 m and between 1800 and 2600 m, respectively.

The sea breeze that develops during the morning reaches the coast between 1000 and 1100 UTC, with the wind veering from southeast to northwest. The sea-breeze front travels inland with a speed of about 10 km h^{-1} and reaches station 348 between 1400 and 1500 UTC.

The onset of the sea breeze at station 348 can be seen very clearly in the profiler measurements (Figs. 3a and 3b). Before the onset of the sea breeze the *U* component

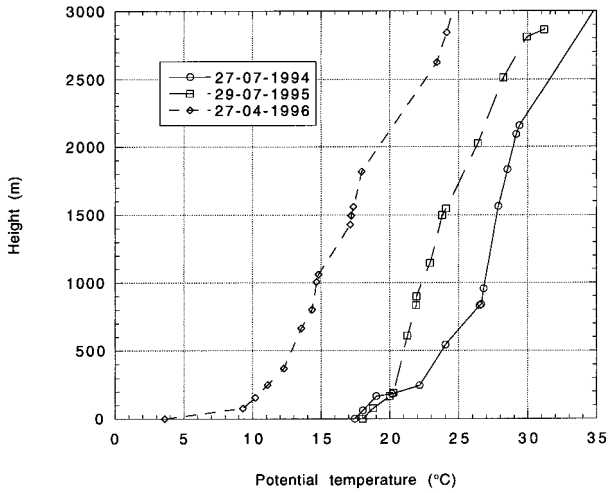

FIG. 2. The initial (0600 UTC) vertical potential temperature profiles for 27 July 1994, 29 July 1995, and 27 April 1996.

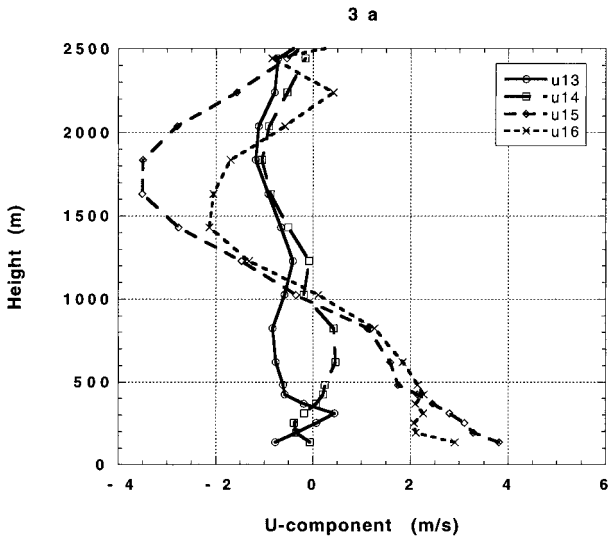

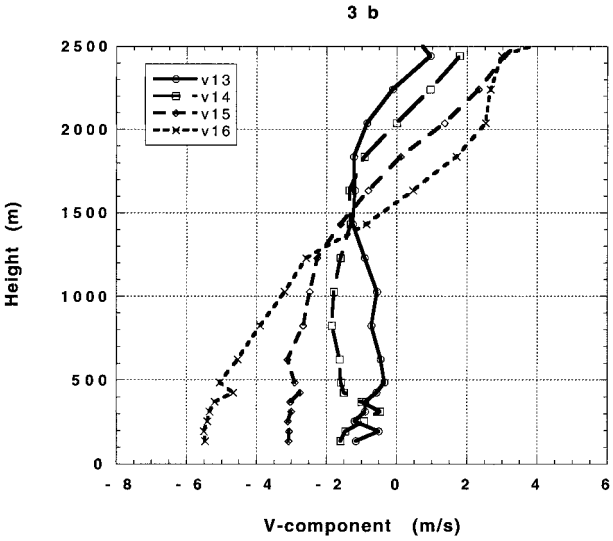

FIG. 3. The vertical profiles of the *U* component (a) and *V* component (b) measured with the profiler at station 348 on 27 April 1996.

of the wind (perpendicular to the coast, see Fig. 1) varies between 0 and 1 m s^{-1} in the layer reaching from the surface up to 2500 m. After the onset of the sea breeze, the *U* component is positive from the surface up to 1000 m. The maximum value is about 4 m s^{-1} at a height of 100 m. Above 1000 m we see the opposite. The *U* component becomes negative with a minimum value of -3.5 m s^{-1} at a height of 1700 m. This is the return current that compensates the sea breeze.

The passage of the sea-breeze front at station 348 can also be deduced from the strong decrease of the *V* component (parallel to the coast, see Fig. 1) after 1400 UTC. Before the sea breeze reaches station 348, the *V* component varies between 0 and -2 m s^{-1} up to a height of 2000 m. After the passage of the sea breeze the *V* component decreases to -3 m s^{-1} at 1500 UTC and -5.5 m s^{-1} at 1600 UTC at a height of about 100 m. Above 100 m the decrease of the *V* component is smaller, turning into an increase at a height of more than 1400 m, well within the layer of the return current.

The return current in this case is extremely well visible in the *U* component. When looking at the difference between 1400 and 1500 UTC, we see that the return current between 1000 and 2300 m entirely compensates the sea breeze below. This is confirmed by looking at the integrated mass fluxes of the sea breeze and the return current.

The integrated mass fluxes of the return current and the sea breeze can be deduced from the vertical profiles of the *U* component. They are calculated by subtracting the *U* component before the onset of the sea breeze from the *U* component after the passage of the sea-breeze front. The differences are integrated over the entire sea-breeze layer or the return current layer. In the presence of a changing large-scale flow the fluxes are calculated from

$$M = \int_{z_1}^{z_2} \{\rho_2(z)[u_2(z) - u_{\text{grad}\,2}(z)] - \rho_1(z)[u_1(z) - u_{\text{grad}\,1}(z)]\}\, dz. \quad (1)$$

Here M is the integrated mass flux perpendicular to the coast (hereafter called the mass flux), ρ the density, u the component of the wind perpendicular to the coast, and u_{grad} the large-scale wind. The subscripts 1 and 2 refer to the profiles before and after the onset of the sea breeze. The large-scale wind can be calculated from the geopotential heights measured with radiosoundings, but

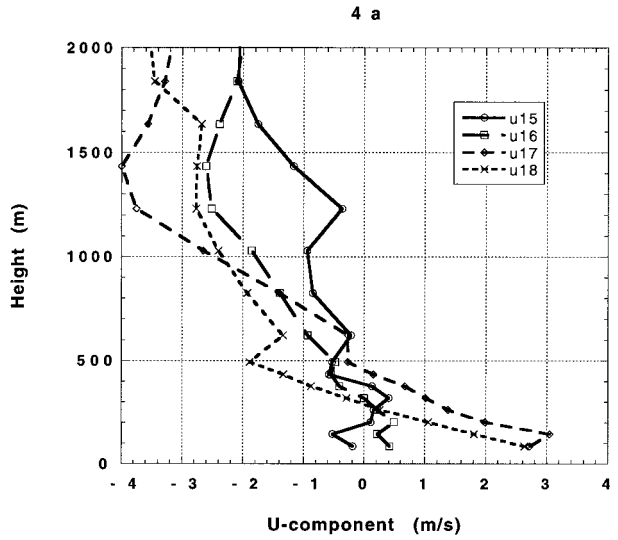

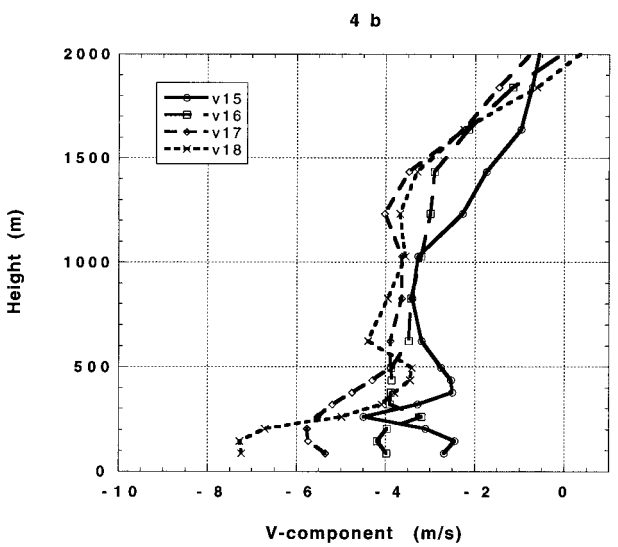

FIG. 4. The vertical profiles of the *U* component (a) and *V* component (b) measured with the profiler at station 348 on 29 July 1995.

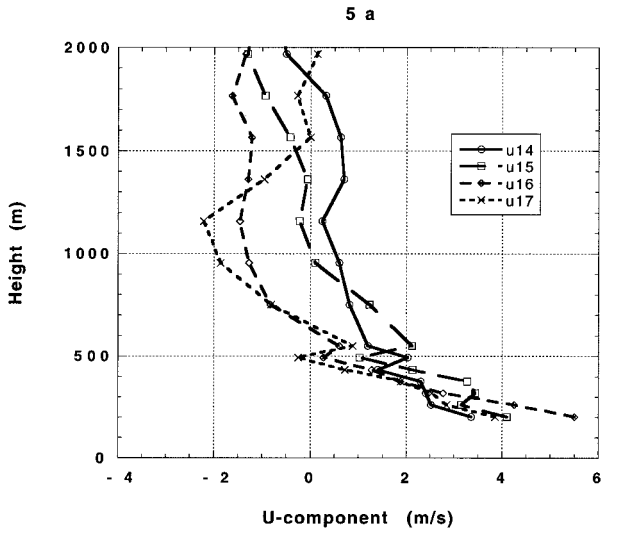

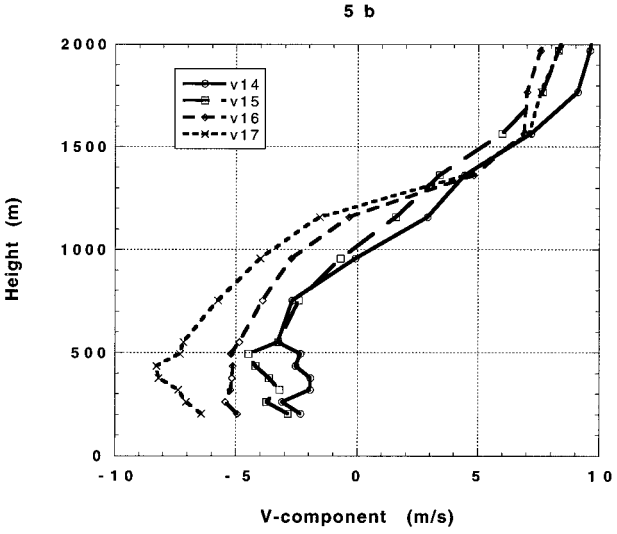

FIG. 5. The vertical profiles of the *U* component (a) and *V* component (b) measured with the profiler at station 348 on 27 July 1994.

the errors in these calculations are a few m s^{-1} (which causes significant errors). A second problem is that the time resolution of the radiosoundings is not sufficient. If the large-scale wind is taken constant in time we have

$$M_a = \int_{z_1}^{z_2} [\rho_2(z)u_2(z) - \rho_1(z)u_1(z)]\, dz. \qquad (2)$$

The result of Eq. (2) is referred to as ''the apparent mass flux,'' whatever the large-scale wind variation in time is. As we have only the wind speed at a limited number of points in the vertical, calculating the mass flux will produce errors (apart from the uncertainty in the profiler measurements). With the method we use (interpolating the wind speed between two points and multiplying with the distance between these points) the mass fluxes are underestimated. A simple experiment with a sinelike wind profile shows that this underestimation depends on the number of points in the layer of which the mass flux is calculated. In the case of 27 April 1996, we have at least eight points both in the return current layer and the sea-breeze layer, implying an error of about 1%. This is much less than the error caused by the uncertainty in the profiler measurements, which is about 0.5 m s^{-1} in this case, causing an uncertainty in the mass

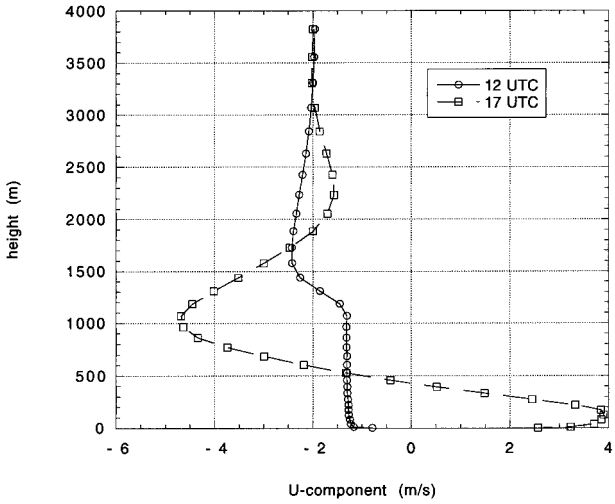

FIG. 6. The simulated vertical profiles of the U component before and after the onset of the sea breeze at 12 km inland. The large-scale U component is -2 m s^{-1}, the initial inversion height is 1000 m, and the temperature jump at the inversion is 6 K.

fluxes of at least 10%. The bias for this type of profiler is shown to be very small (less than 0.15 m s^{-1}; Engelbart et al. 1996).

The apparent mass flux of the sea-breeze layer, computed from Eq. (2) between 1400 and 1500 UTC, is 2.3 $\times$ 10^3 kg m^{-1} s^{-1}, whereas the apparent mass flux of the return current is -2.5×10^3 kg m^{-1} s^{-1}. As the difference between the two mass fluxes is as large as the uncertainty in these fluxes, we conclude that on the basis of the observations the return current approximately compensates the sea breeze. These observations do not rule out the possibility that the return current overcompensates the sea breeze.

From the initial temperature profile it can be seen that the maximum speed of the return current occurs at the top of the pre-sea-breeze boundary layer. The screen height temperature ahead of the sea-breeze front is about 20°C (potential temperature about 18°C), which implies a pre-sea-breeze boundary layer depth of about 1800 m (see Fig. 2). After 1500 UTC the return current decreases in speed more than the sea breeze itself. This decrease is partly caused by the veering of the wind from east to south caused by the Coriolis force, and partly by the approach of a cold front, which causes an increasing southwesterly wind above the boundary layer.

The other two sea-breeze cases will be discussed only briefly, as they served as model validation only. Due to strong time dependence of the large-scale flow these cases cannot be used in the conclusions about the sea breeze and return current mass fluxes. The 0600 UTC vertical temperature profiles can be found in Fig. 2.

On 29 July 1995, the synoptic situation is similar to the situation on 27 April 1996. The differences compared to the first case are the weak flow, opposing the sea breeze, and the smaller daytime sensible heat flux over land. Another difference is that this case occurs in the middle of summer, which means that the sea surface temperature is higher (19°C). As mentioned earlier the large-scale flow, opposing the sea breeze, slowly increases during the day. From geopotential heights measured with radiosoundings in and around the Netherlands it is calculated that the large-scale wind increases by about 4 m s^{-1} from a sea-breeze-opposing direction between 1200 and 2400 UTC. The sea breeze that develops on this day reaches the coast around 1100 UTC. The sea-breeze front moves steadily inland and reaches station 348 between 1600 and 1700 UTC. The passage of the sea-breeze front at station 348 can be seen clearly in the vertical profiles of the wind (Figs. 4a and 4b).

In the third case, 27 July 1994, the initial situation is different from the previous cases. The large-scale U component is positive in the morning and decreases in the afternoon, even more strongly (8 m s^{-1} between 1200 and 2400 UTC) than in the case of 29 July 1995. Because the initial large-scale wind has an onshore component, the sea-breeze front is rather diffuse. The sea surface temperature near the Dutch coast is about 20°C. Surface observations show the diffuse sea-breeze circulation, visible in the wind veering from southwest to northwest in the afternoon. As Coriolis turning is quite important in the Netherlands, the change in the V component is a good indicator of sea-breeze occurrence. Often, the change in the V component is larger than the change in the U component, especially in the case of an onshore flow. The sea breeze travels inland fast. It passes the coast between 1200 and 1300 UTC and reaches station 348 between 1500 and 1600 UTC. The vertical wind profiles (see Figs. 5a and 5b) do not show the onset of the sea breeze at station 348 very clearly, because of a layer with a positive U component of the wind near the ground ahead of the sea breeze. The onset of the sea breeze can be recognized by the strengthening of the V component of the wind after 1500 UTC.

4. Model description

To study the sea breeze and its associated return current, we construct a dry, 2D hydrostatic numerical model. We keep the model and its input as simple as possible to minimize the factors that influence the simulations. In this way we are able to investigate the dynamical structure of the sea-breeze circulation without having to monitor too many parameters. All three cases of sea breeze occur under fair weather conditions with an area of high pressure in the vicinity. Consequently, the drying of the atmosphere occurs due to subsidence, and deep convective clouds do not develop, at least not in the area of interest. Therefore we do not include moisture at this stage.

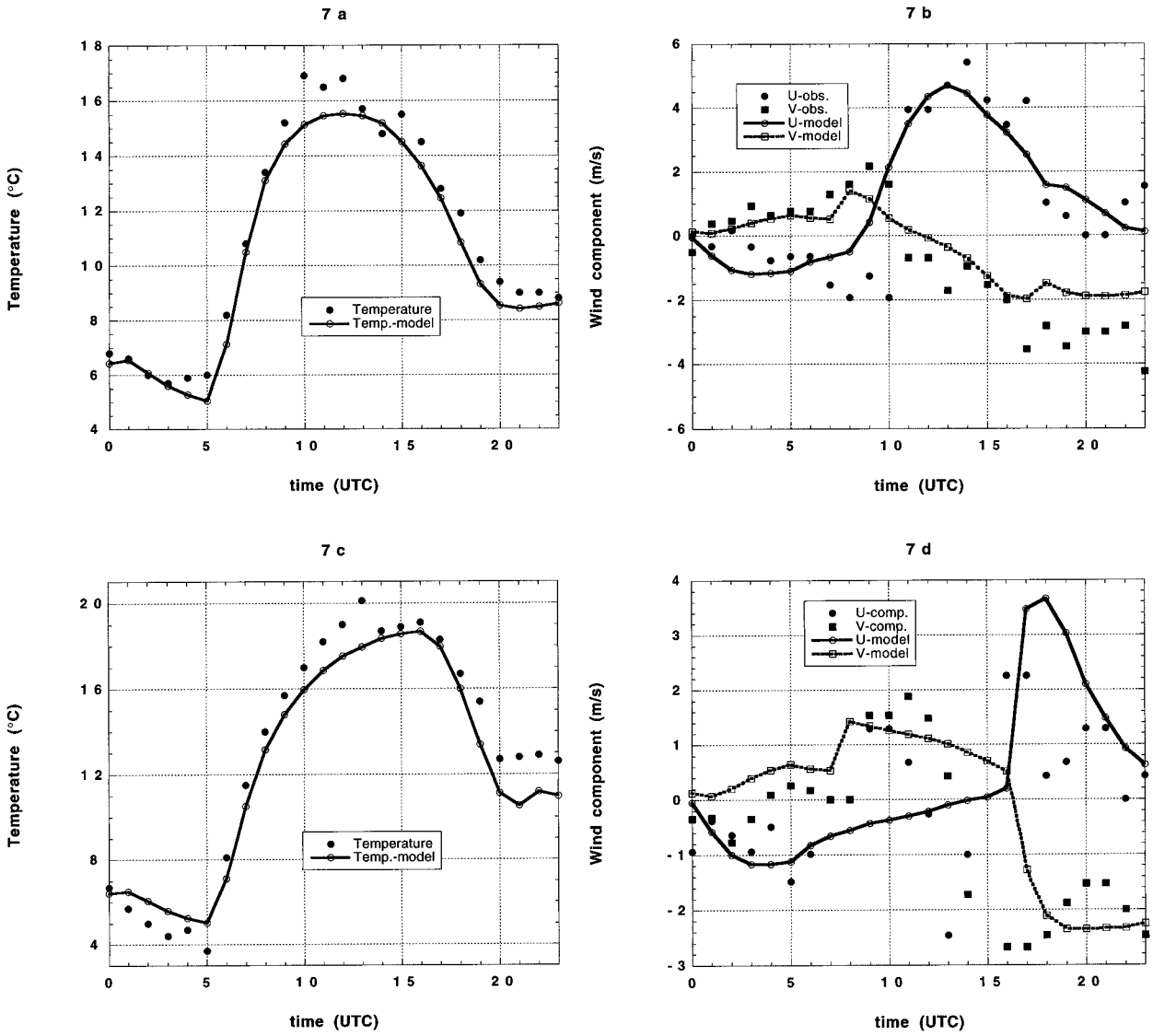

FIG. 7. The surface observations of the temperature and the wind components at station 210 (a) and (b) and station 260 (c) and (d) on 27 April 1996.

a. Basics

Taking the x axis perpendicular to the coast and neglecting all derivatives in the y direction we obtain the following governing equations for a dry atmosphere:

$$\frac{\partial u}{\partial t} + u\frac{\partial u}{\partial x} + w\frac{\partial u}{\partial z} = -\frac{1}{\rho}\frac{\partial p'}{\partial x} + f(v - v_g) - \frac{\partial}{\partial z}(\overline{u'w'}), \quad (3)$$

$$\frac{\partial v}{\partial t} + u\frac{\partial v}{\partial x} + w\frac{\partial v}{\partial z} = -f(u - u_g) - \frac{\partial}{\partial z}(\overline{v'w'}), \quad (4)$$

$$\frac{\partial \rho u}{\partial x} + \frac{\partial \rho w}{\partial z} = 0, \quad (5)$$

$$\frac{\partial \theta}{\partial t} + u\frac{\partial \theta}{\partial x} + w\frac{\partial \theta}{\partial z} = -\frac{\partial}{\partial x}(\overline{u'\theta'}) - \frac{\partial}{\partial z}(\overline{w'\theta'}), \quad (6)$$

$$\frac{\partial p}{\partial z} = -\rho g \quad \text{with } \rho = \frac{p}{RT}. \quad (7)$$

Here, u, v, and w are the three wind components in the x, y, and z direction, respectively; θ is the potential temperature; T is the temperature; ρ is the density; R is the gas constant for dry air; f the Coriolis parameter; g the gravity force; p' is the pressure perturbation $[p'(z, t) = p(z, t) - p(z, 0)]$ calculated with the hydro-

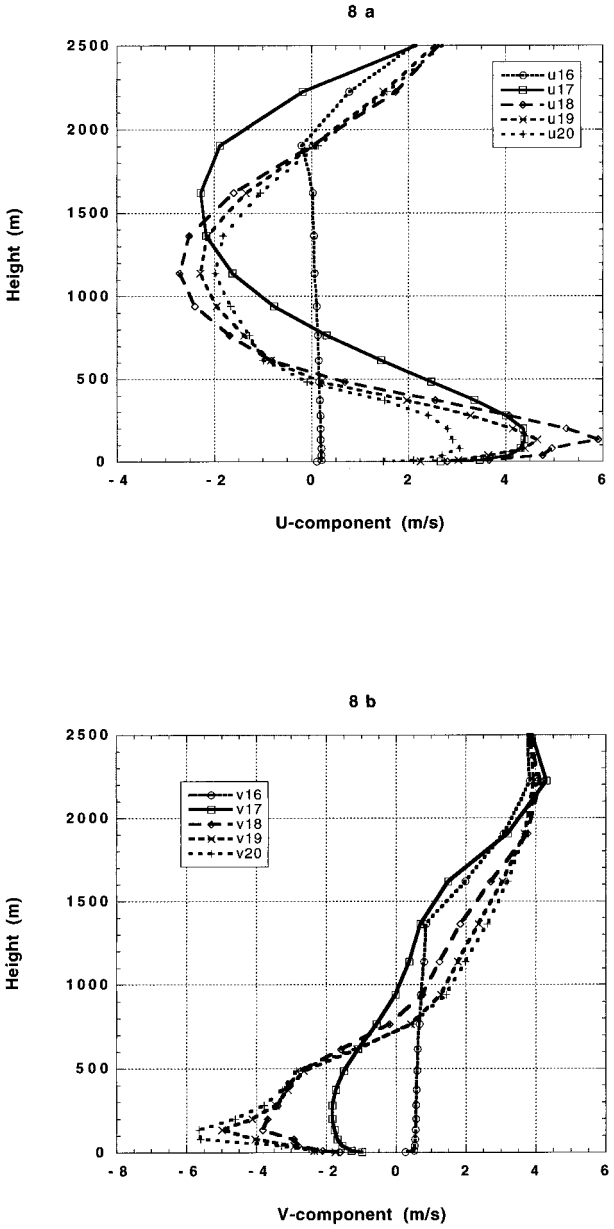

FIG. 8. The vertical profiles of the *U* component (a) and *V* component (b) simulated with the model on 27 April 1996.

static equation from the model top downward [see Eq. (7)]; and u_g and v_g are the large-scale geostrophic components of the wind. The pressure is split into a large-scale part represented by fu_g and fv_g and a perturbation (calculated hydrostatically) caused by the differential heating. The last terms in Eqs. (3) and (4) are the vertical turbulent momentum fluxes, whereas the last term in Eq. (6) is the vertical turbulent sensible heat flux. These cannot be calculated directly from the values on the model grid but must be parameterized. The vertical component of the wind is calculated from the 2D continuity equation [Eq. (5)].

To parameterize the turbulent sensible heat flux we use a nonlocal diffusion scheme, which is described in detail in Holtslag and Boville (1993). This scheme includes a nonlocal transport term, which reflects the mixing of the largest and strongest eddies. In the calculation of the potential temperature the nonlocal transport term is historically known as the countergradient term. The formulation for the turbulent momentum fluxes takes the form of a K formulation. For more details of these parameterizations and the handling of the horizontal diffusion we refer to the appendix.

On the landward side of the coast the turbulent sensible heat flux is prescribed during the daytime. The total surface sensible heat flux is estimated from the temperature profile at De Bilt at 0600 GMT and the maximum temperature of a few stations farther inland. This amount of heat is added to the air over land in the model during the daytime with a zero flux at sunrise plus 1 h and sunset minus 1 h. In between these hours we apply positive values with a sinelike time dependence. At night the sensible heat flux is parameterized. For a comprehensive description of this parameterization we refer to Van Ulden and Holtslag (1985). The sea surface temperature is kept constant during the integration period.

b. Numerics and inputs

The primitive equations are solved on a staggered model grid. The model domain consists of an inner model domain that has a constant gridpoint distance and two boundary domains in which the grid distance increases toward the lateral boundaries. The inner model domain extends from 60 km out to sea to 90 km inland (see Fig. 1). With a horizontal grid spacing of 3 km, this means that we have 51 grid points in the horizontal direction in the inner model domain. The grid distance between the outmost 10 points in the horizontal direction is doubled after every point. This procedure puts the lateral boundaries far (more than 3000 km) away from the inner grid points. This prevents boundary reflections from interfering with the solution on the points of interest in the center of the model domain. Therefore the total number of horizontal grid points is 71. As lateral boundary condition we impose fixed horizontal gradients.

In the vertical direction, there are 25 grid points. In most cases the sea breeze reaches a maximum height of about 500 m. The steepest gradients in the temperature and the wind are usually found near the ground or in the lowest few hundred meters of the atmosphere. Therefore, the model has a better resolution close to the ground in the area where the sea breeze occurs, that is, up to a height of about 1500 m. The model resolution decreases from 50 m above the surface layer to about 200 m at a height of 2000 m. The model top lies at a height of about 6100 m, well above the maximum vertical extent of the sea breeze and the accompanying

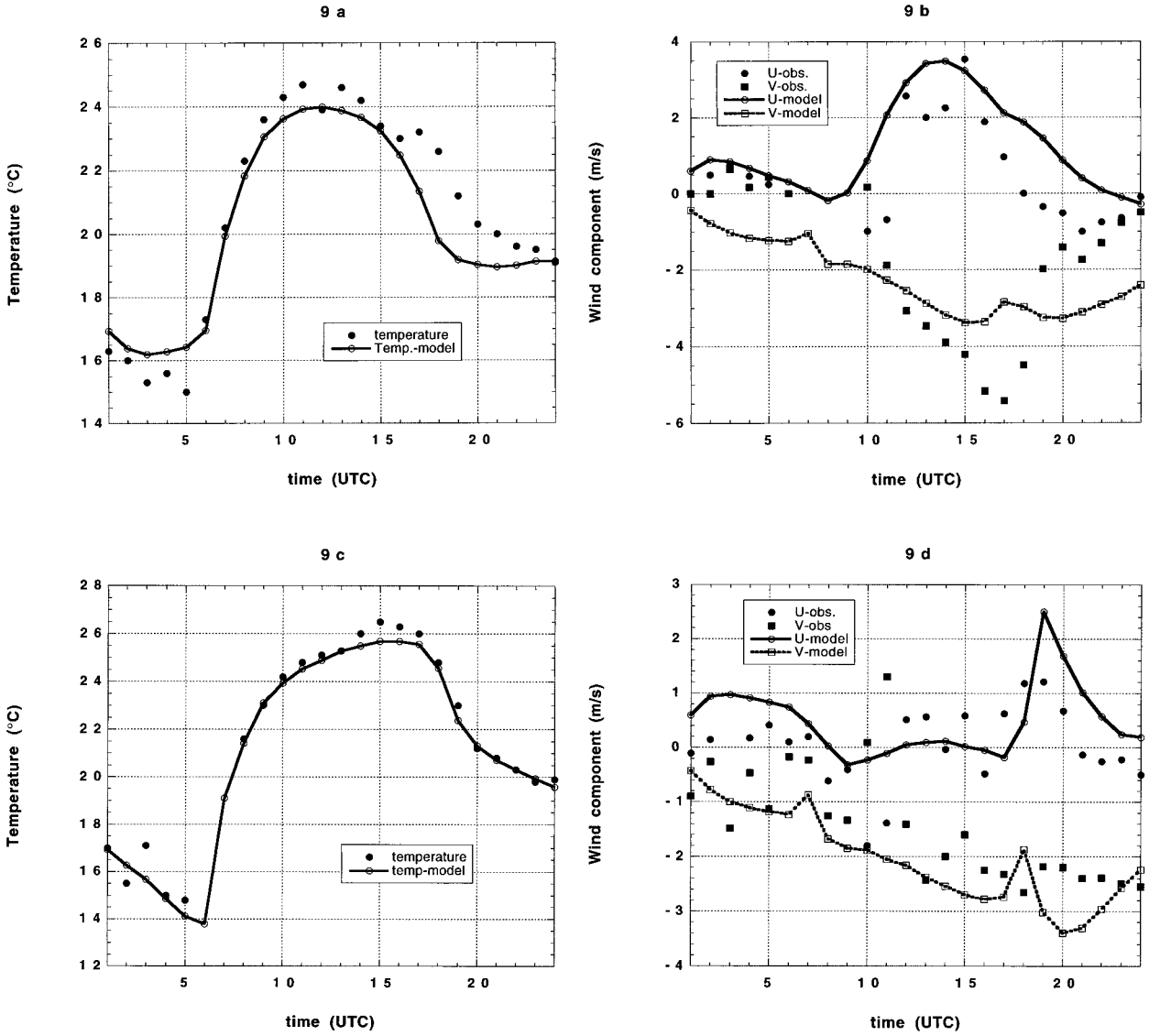

FIG. 9. The surface observations and simulation of the temperature and the wind components at station 210 [(a) and (b)] and station 348 [(c) and (d)] on 29 July 1995.

return current. At the model top we impose a fixed pressure and fixed vertical gradients for all the other parameters.

We use a semi-implicit scheme with an upstream scheme for the advection terms. Because of the small time step of 25–50 s, the upstream advection scheme works well. The diffusive character enhances the computational stability and it prevents over- and undershooting near steep temperature gradients. To warrant computational stability, the vertical diffusion is calculated in smaller time steps, which satisfy the standard nonlinear stability criterion when necessary. To ensure stability, we also introduce horizontal diffusion in our model (see the appendix).

To initialize the model, we use the temperature and wind profiles obtained at De Bilt (see Fig. 2) at 0600 UTC. The initial grid values for temperature, pressure, and momentum are calculated from the observed profiles by linear interpolation. The entire model domain is initialized horizontally homogeneous with the vertical profiles obtained in this way.

It is possible to account for changing large-scale meteorological conditions. If the large-scale wind changes significantly during the integration period, which can be seen from the profiles of the wind measured at De Bilt and calculated from the geopotential heights measured at a number of stations in and surrounding the Netherlands, we alter the large-scale components of the wind gradually at all model points by an amount that corresponds to these profiles. By doing so, the large-scale wind remains horizontally homogeneous.

As this study concentrates on the vertically integrated

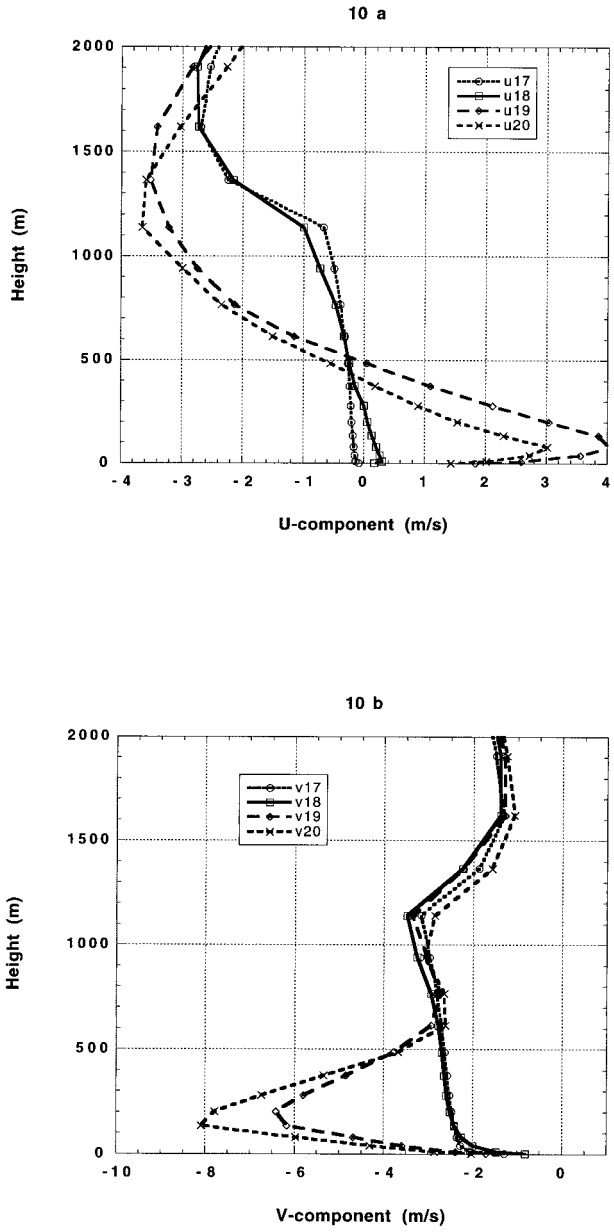

FIG. 10. The vertical profiles of the *U* component (a) and *V* component (b) simulated with the model on 29 July 1995.

mass fluxes it is important to know if the mass fluxes are properly simulated. To gain confidence in the model we have made a control run starting from rest. The integrated vertical profiles of the wind show that the amount of mass moving in one direction is compensated by the same amount of mass moving in the other direction at all model points. Therefore the vertically integrated horizontal mass flux is zero and mass is conserved. This can also be illustrated by taking vertical profiles of the *U* component of the wind before and after the onset of the sea breeze from one of the runs of the sensitivity study we will perform in section 6 (see Fig. 6). It clearly shows the return current with a larger mass flux than the sea breeze. This is compensated by a landward-directed flow above the return current layer, which can be named ''return–return current.''

5. Model results

We have used the model described in the previous section to simulate the cases described in section 3. Because we are most interested in the vertical structure of the sea breeze and the accompanying return current, we will focus on this aspect when comparing the model simulations with the observations. Note that typically events near the surface are reproduced quite well (see Figs. 7a–d, 9a–d, and 11a–d). The largest deviations that occur are about 2°C for the 2-m temperature, 2 m s^{-1} for the 10-m wind components, and about 2 h for the time of onset of the sea breeze at station 348. However, most of the time the deviations are smaller than the values mentioned above.

The simulated vertical profiles of the wind components of the case of 27 April 1996 compare well with the observed profiles (cf. Figs. 8a and 8b with Figs. 3a and 3b). The simulated sea breeze is 2 m s^{-1} too strong at a height of 100 m with a sea-breeze layer that is too shallow. The decrease in time of the *V* component in the sea-breeze layer as well as the increase above the sea-breeze layer is simulated correct qualitatively.

The simulated *U* component of the wind in the return current is too weak, although the profile has the same shape as observed. The simulated mass fluxes, which are computed by comparing the vertical profiles of the *U* component before and after the onset of the sea breeze [see Eq. (2)], also compare well with the observations. The simulated mass flux in the sea-breeze layer at station 348 (1500–1700 UTC) is 2.4×10^3 kg m^{-1} s^{-1} against 2.3×10^3 kg m^{-1} s^{-1} observed. The simulated mass flux in the return current layer (-2.5×10^3 kg m^{-1} s^{-1}) is in accordance with the observations. An important conclusion from this case is that the mass flux of the return current is about 5% larger than that of the sea-breeze layer in the simulation, whereas this effect is not ruled out by the observations. The simulated overcompensation is larger than the error in the calculation of this overcompensation (about 1%), which enhances the confidence in the simulated overcompensation and the possibility that this is a real physical phenomenon.

As we use the second and third sea-breeze cases only to validate the model, these cases will be discussed only briefly. The observed and simulated wind profiles at station 348 in the second case (29 July 1995) compare well (cf. Figs. 10a and 10b with Fig. 4a and 4b). The simulated sea breeze has its maximum strength at the same height as observed, but it is 1 m s^{-1} stronger. The depth of the simulated sea-breeze layer is as observed. The simulated return current reaches a maximum strength of -3.5 m s^{-1} at the same height as observed,

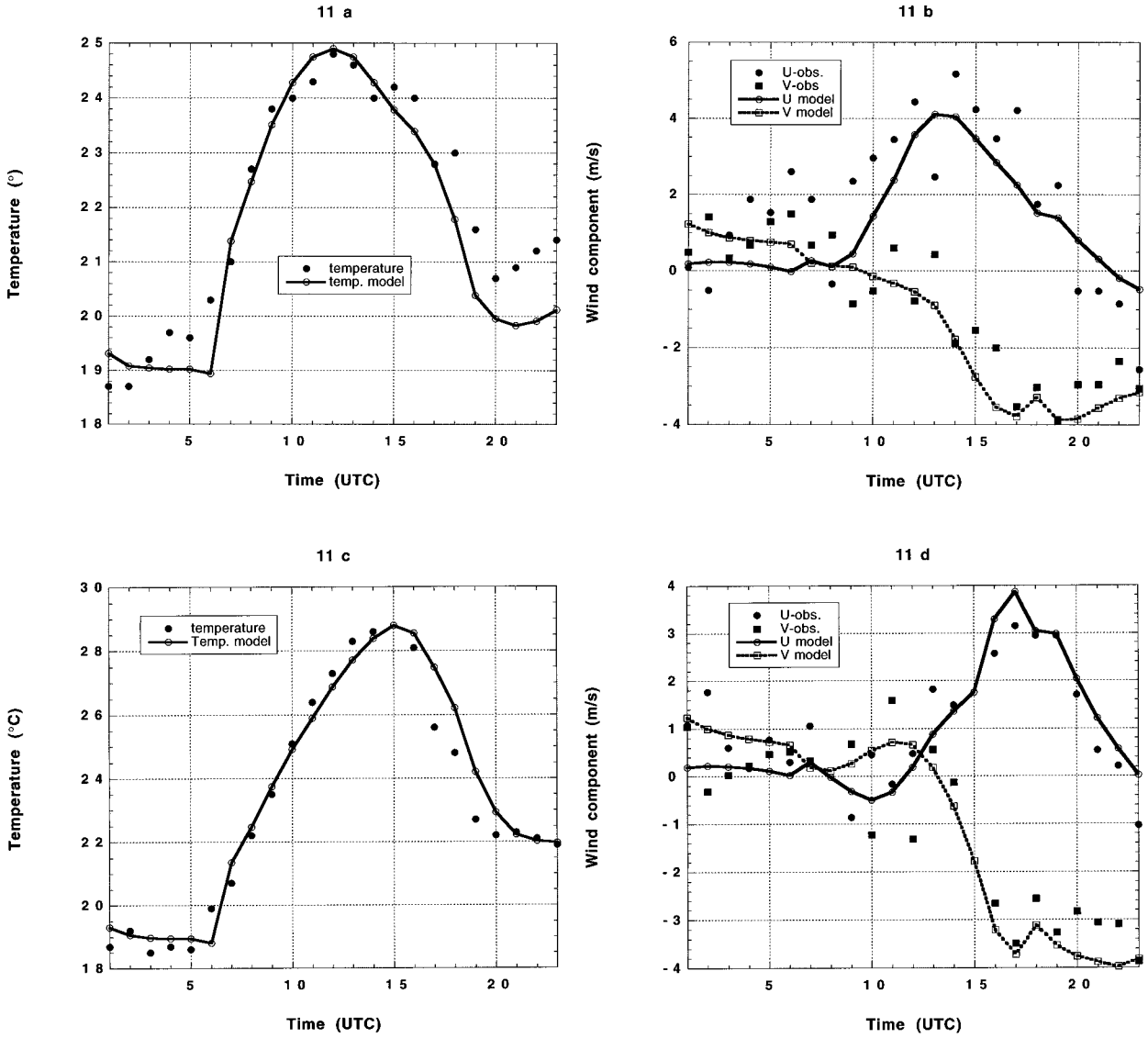

FIG. 11. The surface observations and simulation of the temperature and the wind components at station 210 [(a) and (b)] and station 348 [(c) and (d)] on 27 July 1994.

but it is 0.5 m s^{-1} weaker than the observed maximum strength.

In the simulation of the third case, 27 July 1994, the maximum observed *U* component in the sea-breeze layer at station 348 is about 1 m s^{-1} larger than simulated (cf. Figs. 12a and 12b with Figs. 5a and 5b). The deviations in the *V* component are larger by up to 3 m s^{-1} in the sea-breeze layer. The depth of the sea-breeze layer is between 300 and 400 m in the observations and about 500 m in the simulation. The shape and strength of the simulated and observed return current are similar.

6. Understanding the return current

In the ideal case of 27 April 1996, with no change in the large-scale conditions, the observed return current mass flux approximately equals the sea-breeze mass flux, whereas the simulated mass flux of the return current is 5% larger than that of the sea breeze.

Because the observed relative mass fluxes compare well with the simulations, it is justified to look at the simulation to try and find an explanation for the excess of the return current mass flux. With the convergence at the sea-breeze front, relatively cool air is transported upward, whereas subsidence behind the sea-breeze front transports relatively warm air downward. From different model runs it is clear that this results in a differential heating of the air in the layer of the return current. The unperturbed return current, that is, the return current that compensates the sea breeze, is caused by continuity. The pressure gradients caused by the updrafts near the sea-breeze front and the subsidence behind the sea-

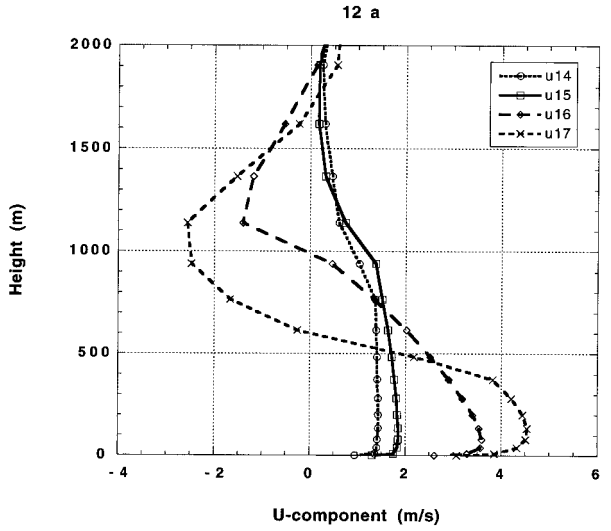

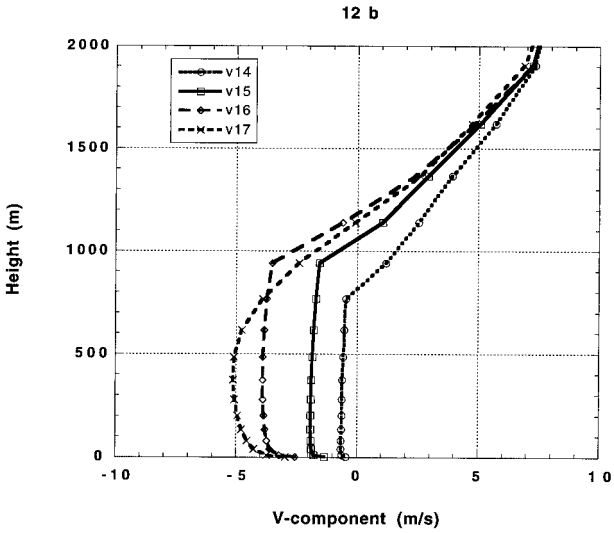

FIG. 12. The vertical profiles of the *U* component (a) and *V* component (b) simulated with the model on 27 July 1994.

breeze front can enhance the return current to a level where it exceeds the sea breeze.

When looking at the mass fluxes and keeping in mind that the two-dimensional continuity equation has to be satisfied, one could ask, Where does the extra air in the return current go or come from? In the observations there is no evidence of a compensation for this effect, because the measurements were only available up to 2500 m, the depth of the sea-breeze circulation. However, the simulations show that above the return current there is a layer with a deviation from the large-scale wind in the direction of the sea breeze (see Fig. 6). This

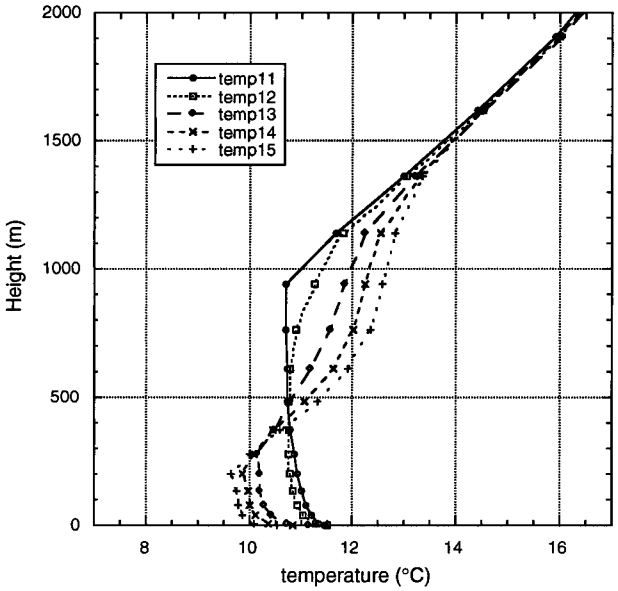

FIG. 13. The simulated vertical profiles of the temperature between 1100 and 1500 UTC, 12 km inland from the coast, with an initial vertical potential temperature gradient of 5 K km^{-1} and a vertical wind gradient of -5 m s^{-1} km^{-1}.

is a very weak effect, with the deviation of the wind from the large-scale wind being about 0.5 m s^{-1}. It will probably be very difficult to find conclusive evidence of this effect in observations.

To try and find evidence of the heating of the air in the return current layer, we perform an experiment in which we assume an initial atmosphere with a potential temperature that increases with 5 K km^{-1} in the vertical direction and a large-scale *U* component decreasing linearly from 0 m s^{-1} at the surface to -10 m s^{-1} at a

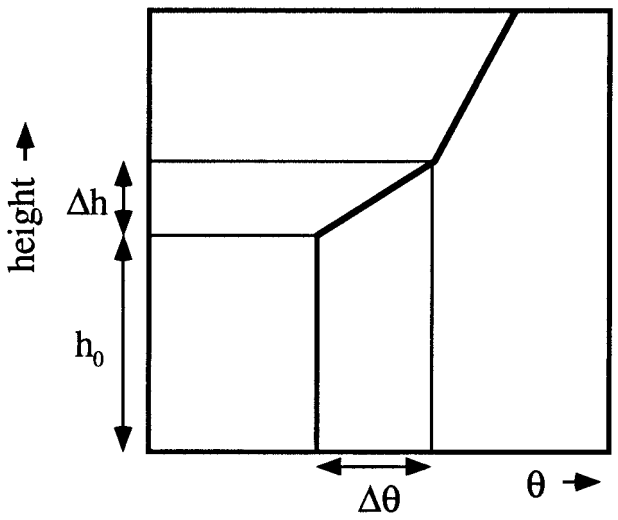

FIG. 14. Conceptual plot of the initial conditions in the sensitivity study. The initial height of the boundary layer is h_0, the initial temperature jump is $\Delta\theta$, and the initial depth of the inversion is Δh.

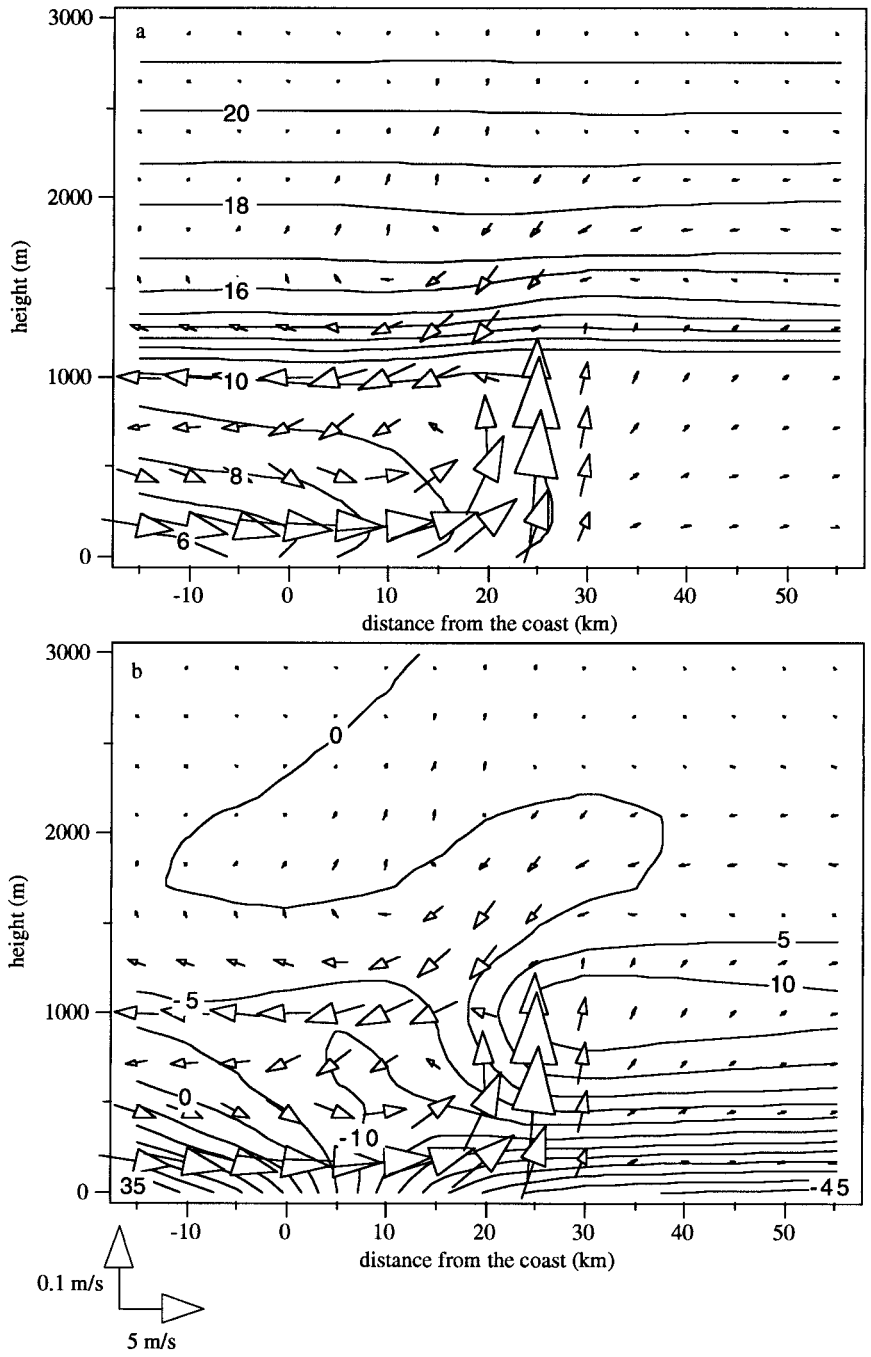

FIG. 15. The 2D wind field minus the large-scale flow (w multiplied by 50) together with the potential temperature distribution (a) (contour interval °C) and the pressure perturbation from the horizontal average pressure (b) (contour interval 5 Pa) at 1600 UTC for the case with an initial boundary layer height, h_0, of 1000 m, and an initial inversion strength, $\Delta\theta$, of 10 K.

height of 2000 m. Figure 13 displays the temperature profiles from 1100 to 1500 UTC at a model point over land that lies 12 km from the coast. The sea breeze reaches this point between 1100 and 1200 UTC. After the onset of the sea breeze the temperature slowly drops at the surface and in the sea-breeze layer. The boundary layer height drops from about 1000 m before the onset of the sea breeze to about 280 m at 1300 UTC and 200 m at 1500 UTC. Above the sea-breeze layer the temperature increases. This increase cannot be caused by sensible heating from the surface upward because the (internal) boundary layer is too shallow. The increasing

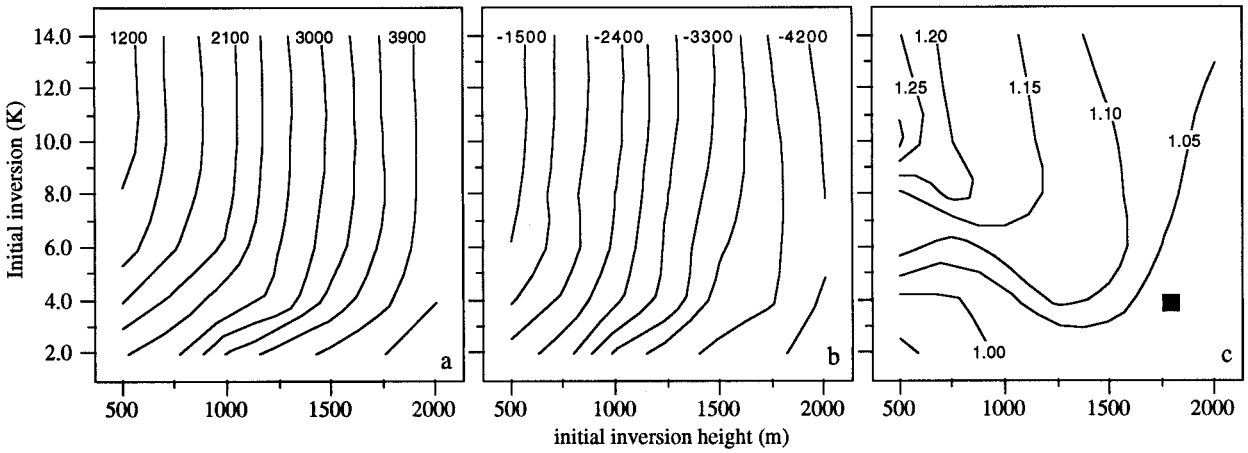

FIG. 16. The sea-breeze mass flux (a) (contour interval 300 kg s^{-1}), the return current mass flux (b) (contour interval 300 kg s^{-1}), and the absolute ratio of the return current mass flux and the sea-breeze mass flux (c) (contour interval 5%) for an initial boundary layer height (h_0) ranging from 500–1500 m and an initial inversion strength ($\Delta\theta$) ranging from 2 to 14 K. The black square in (c) represents the conditions on 27 April 1996.

temperature must therefore be the result of downward advection of warm air.

The simulations discussed above suggest that the amount of overcompensation by the return current depends upon the vertical advection of warm air and upon the boundary layer height. Therefore we investigate the sea-breeze circulation in the model as a function of the initial depth of the boundary layer (h_0, see Fig. 14) and the initial strength of the inversion ($\Delta\theta$, 0600 UTC). Above the inversion the potential temperature increases with 3.5 K km^{-1}. In all runs we keep the large-scale wind at -2 m s^{-1} and the daytime average sensible heat flux at the surface at 127 W m^{-2} with a maximum value of 200 W m^{-2} at 1200 UTC, whereas the inversion has a fixed initial depth of 250 m (Δh).

To clarify the mechanism that initiates and enhances the return current, we have plotted some 2D fields from one of the model runs of the sensitivity study. Figures 15a and 15b show the 2D wind field minus the large-scale flow of -2 m s^{-1} at 1600 UTC together with the potential temperature distribution (a) and the pressure perturbation from the horizontal averaged pressure (b). The initial boundary layer depth over land is 1000 m and the initial inversion strength is 10 K. The wind field shows the sea-breeze circulation with the sea-breeze front positioned between 20 and 30 km inland. The strongest positive vertical wind speed is located near the front at a height of 750 m, and the region with the strongest subsidence is located behind the sea-breeze front near the bottom of the inversion at a height of 1250 m.

The vertical motions have an important impact upon the temperature field. On the landward side of the sea-breeze front the isentropes are raised at the top of the boundary layer. Behind the sea-breeze front, in the region of the strongest subsidence, the opposite is the case. Due to this, a positive pressure perturbation develops at the top of the boundary layer on the landward side of the sea-breeze front (see Fig. 15b). The subsidence behind the sea-breeze front causes a negative pressure perturbation. The resulting pressure gradient enhances the return current. The pressure perturbation gradient that causes the enhancement of the return current will be a function of the warming behind and the cooling in advance of the sea-breeze front, which in turn will be a function of the vertical temperature distribution and the strength of the vertical motions near the sea-breeze front.

Above the return current, between 0 and 20 km inland and at a height of about 2000 m, positive vertical velocities are observed (see Fig. 15a). These cause a slight cooling of this layer, resulting in a small positive pressure perturbation. The resulting weak pressure gradient causes a weak relative flow in the direction of the sea breeze, referred to as the return–return current.

The results of the sensitivity experiment show that the mass flux of the sea breeze increases with increasing boundary layer depth (see Fig. 16a). The increase of the sea-breeze mass flux with decreasing initial inversion strength is associated with the clearing of the inversion when it is very weak. When the inversion is cleared, the boundary layer increases more in depth than when the inversion is not cleared, resulting in a deeper sea-breeze layer and a larger mass flux of the sea breeze. The return current shows a similar behavior (see Fig. 16b). However, for the major part of the range of initial conditions the return current mass flux is about 300 kg m^{-1} s^{-1} larger than the sea-breeze mass flux.

The ratio of the mass flux of the return current and the mass flux of the sea breeze is plotted in Fig. 16c. We note that when the inversion above the boundary layer is strong enough, the mass flux of the return current is larger than that of the sea breeze. The largest relative difference occurs for a shallow boundary layer and an

inversion strength of about 10°C. With a deeper boundary layer the relative difference becomes smaller, but the absolute difference (sea-breeze mass flux minus return current mass flux) remains the same.

The ratio between the return current mass flux and the sea-breeze mass flux is less than one in the case of a weak initial inversion and a relatively shallow boundary layer. In these cases the inversion is cleared before the sea breeze arrives at the model point used in the sensitivity study. Above the initial inversion the air is also stable, but the vertical potential temperature gradient is smaller. This means that the warming of the air behind the sea-breeze front by subsidence is less than in the case of a strong inversion that is intact at the moment of passage of the sea-breeze front. This results in smaller pressure perturbations in the return current layer and a weaker return current.

In the case of 27 April 1996, the return current mass flux approximately compensates the sea-breeze mass flux. These observations do not rule out the possibility of a return current overcompensation, which is 5% in the simulation of this day. As the pre-sea-breeze boundary layer has a depth of about 1800 m and the inversion has a strength of 6 K $(700\ \text{m})^{-1} \sim 2$ K $(250\ \text{m})^{-1}$, this possible overcompensation can be compared with the values found in the sensitivity study (black square in Fig. 16c). The square has been plotted at the initial inversion of 4 K (and not at 2 K) because in the sensitivity study the inversion has weakened by about 2 K at the moment of passage of the sea-breeze front whereas it is intact in the observations. According to the sensitivity study, the return current has an overcompensation of 4%, which agrees with the simulation of this case.

As the simulated mass flux in one direction must be compensated by the same mass flux in the other direction, the overcompensation by the return current must be compensated by a flow in the direction of the sea breeze above the return current. In all simulations with a larger return current mass flux, this compensating flow can be found. The mass flux of this return–return current entirely compensates the overcompensation of the return current.

The return–return current can be found in other simulations of the sea breeze [i.e., see Fig. 6 left, Mahrer and Pielke (1977); Fig. 3, Physick (1980); and more recently, Fig. 1, Sha et al. (1993); Fig. 8, Lu and Turco (1994); and Fig. 4 and 5 in Koo and Reible (1995b)]. It is probably due to the weak nature of the return–return current and the attention that was focused on the sea breeze itself that it has not received attention before.

7. Conclusions

All three sea-breeze cases presented in this study produce return currents. In two of the cases the apparent return current mass flux is much larger than that of the sea breeze. This effect is caused by the strengthening in time of the opposing large-scale flow, which produces large errors in the calculation of the mass fluxes. In the case of 27 April 1996, the large-scale flow, is rather weak and constant in time. In this case, the observed return current mass flux approximately equals the observed sea-breeze mass flux, whereas the simulated return current mass flux is larger than the simulated mass flux of the sea breeze.

Although we use a fairly simple model, the simulations of the three sea-breeze cases are qualitatively in accordance with the observations, not only for the sea breeze itself, but also for the accompanying return current.

A sensitivity study of the return current with the numerical model shows that the return current mass flux is larger than the sea-breeze mass flux, when the vertical potential temperature gradient above the pre-sea-breeze boundary layer is larger than the initially imposed vertical potential temperature gradient above the inversion. When the inversion is cleared, the prefrontal cooling and the warming behind the front by vertical advection of heat is too small to cause pressure perturbations at the return current level that enhance the return current.

The maximum relative overcompensation is about 30% in the case of a shallow initial boundary layer and a strong initial inversion. The relative importance of the overcompensation decreases with increasing boundary layer depth.

The overcompensation by the return current is compensated by a return–return current. As this return–return current is very weak and often lies above 2000 m it will be very difficult to find it in observations.

Acknowledgments. The observations used in this study were kindly provided by the Royal Netherlands Meteorological Institute (KNMI). We would especially like to thank Henk Klein Baltink for providing the measurements made with the wind profiler at Cabauw, and Gerard van der Vliet for providing the observations made at the 200-m meteorological tower at Cabauw. Dr. Peter Bechtold and three unknown referees are acknowledged for critically reading the manuscript and their useful comments.

APPENDIX

Boundary Layer Fluxes

a. Parameterization of the sensible heat flux

To parameterize the sensible heat flux we use a nonlocal diffusion scheme, which is described in detail in Holtslag and Boville (1993) and Holtslag et al. (1995). The flux of sensible heat is described by

$$(\overline{w'\theta'}) = -K_\theta\left(\frac{\partial\theta}{\partial z} - \gamma_\theta\right). \tag{A1}$$

In Eq. (A1), K_θ is the eddy diffusivity for the potential

temperature, $(\partial\theta/\partial z)$ is the local potential temperature gradient, and γ_θ is the countergradient term. The eddy diffusivity K_θ is given by

$$K_\theta = kw_t z\left(1 - \frac{z}{h}\right)^2, \quad \text{(A2)}$$

where k is the von Kármán constant (=0.4), w_t is the turbulent velocity scale for mixing of passive scalars, z is the height, and h is the height of the boundary layer. The countergradient term in Eq. (A1) is given by

$$\gamma_\theta = a\frac{w_*(\overline{w'\theta'})_s}{w_m^2 h}, \quad \text{(A3)}$$

where $(\overline{w'\theta'})_s$ is the sensible heat flux at the surface, w_m is the turbulent velocity scale for the mixing of momentum, a is a constant (=7.2), and w_* is the convective velocity scale that represents the strength of the eddies as a function of the sensible heat flux at the surface. When the surface sensible heat flux is negative, γ_θ is set to zero (stable conditions).

The eddy diffusion coefficient [Eq. (A2)] and the countergradient term [Eq. (A3)] are a function of the boundary layer height. The boundary layer height, the height reached by the most powerful eddies, is calculated iteratively from

$$h - z_1 = \frac{\mathrm{Ri}_{\mathrm{cr}}[(u_h - u_1)^2 + (v_h - v_1)^2]}{(g/\theta_s)(\theta_h - \theta_s)}, \quad \text{(A4)}$$

where $\mathrm{Ri}_{\mathrm{cr}}$ is the critical Richardson number [=0.25, taken from Holtslag et al. (1995)]. All values with the subscript h are calculated at the boundary layer height, all values with the subscript 1 are taken at the lowest model level, and all values with the subscript s are surface values.

Because the diffusion scheme described above is valid only in the boundary layer, a second diffusion scheme is used to calculate diffusion above the boundary layer. This is a local diffusion scheme that uses the normal K parameterization (see Holtslag and Boville 1993). In this scheme K_θ is defined by

$$K_\theta = l_\theta^2 S F_\theta(\mathrm{Ri}). \quad \text{(A5)}$$

In Eq. (A5) l_θ is a mixing length scale, S is the vertical wind shear, and $F_\theta(\mathrm{Ri})$ is a function of the gradient Richardson number (see Holtslag and Boville 1993). The function $F_\theta(\mathrm{Ri})$ becomes very small for Richardson numbers larger than 1. This causes the vertical turbulent mixing of heat to become almost zero if Ri is larger than 1. As a result there is too strong cooling near the surface, which in turn increases stability and thereby the Richardson number. To prevent this from occurring, the function is cut off at its minimum, which is achieved for Richardson numbers larger than 1. The length scale l_θ is given by

$$\frac{1}{l_\theta} = \frac{1}{kz} + \frac{1}{\lambda_\theta}, \quad \text{(A6)}$$

where k is the von Kármán constant, z is the height, and λ_θ is an asymptotic length scale (approaching 30 m asymptotically above the boundary layer).

Eddy diffusivities according to Eqs. (A2) and (A5) are both calculated in the boundary layer. The larger one is used to calculate the fluxes. In this way a smooth transition between the calculation of the fluxes in and above the boundary layer is created and instabilities caused by sharp steps are avoided, especially at the top of the boundary layer and at the transition from a deep daytime boundary layer toward a shallow nighttime one.

Above the land the sensible heat flux is prescribed during the day and parameterized during the night (Van Ulden and Holtslag 1985). Over the sea the surface sensible heat flux is parameterized with a drag law as

$$(\overline{w'\theta'})_s = -C_\theta(\theta_s - \theta_1)u_1. \quad \text{(A7)}$$

In Eq. (A7), the subscript s refers to the values at the surface, subscript 1 to values at the lowest model level, and C_θ is the surface exchange coefficient, which consists of a neutral part and a part that is a function of the stability.

By means of Eqs. (A1)–(A7) the sensible heat flux for all model layers is calculated. Then the temperature tendencies arise from the divergence of the sensible heat flux. For a comprehensive overview of the quantities that are not discussed in this paper [a, w_m, w_t, w_*, and $F_\theta(\mathrm{Ri})$] the reader is referred to Holtslag and Boville (1993) and Holtslag et al. (1995).

Finally, the horizontal diffusion of heat is calculated with a K parameterization with the horizontal diffusion coefficient defined by

$$K_H = \alpha w_m(\Delta x), \quad \text{(A8)}$$

where α is 0.25 and w_m the turbulent velocity scale.

b. Parameterization of the momentum flux

For the momentum flux a local scheme is used. The format of this scheme resembles the heat flux scheme but does not involve a nonlocal transport term. The parameterization takes the form of a K formulation and is described by

$$(\overline{u'w'}) = -K_m\left(\frac{\partial u}{\partial z}\right), \quad \text{(A9)}$$

where K_m is the eddy diffusion coefficient for momentum, which is defined in the same way as the eddy diffusion coefficient for sensible heat, except for the fact that w_t is replaced by w_m, the turbulent velocity scale for momentum. Here K_m is given by

$$K_m = kw_m z\left(1 - \frac{z}{h}\right)^2. \quad \text{(A10)}$$

In Eq. (A10) we define the eddy diffusion coefficient within the boundary layer. Above the boundary layer K_m is defined by

$$K_m = l_m^2 S F_m(\mathrm{Ri}), \tag{A11}$$

where l_m is an asymptotic length scale, S is the vertical wind shear, and $F_m(\mathrm{Ri})$ is a function of the Richardson number. This function is also minimized for Richardson numbers larger than 1. The length scale l_m is defined in the same way as l_θ. For a discussion of $F_m(\mathrm{Ri})$, we refer to Holtslag and Boville (1993). Using Eqs. (A9)–(A11) it is possible to calculate the momentum flux in the entire model domain. The momentum flux at the ground acts as a boundary condition and is calculated with a drag law:

$$(\overline{u'w'})_s = -C_M |V_2| u_2. \tag{A12}$$

In Eq. (A12) $(\overline{u'w'})_s$ is the momentum flux at the ground, V_2 is the wind speed at the second model level, and C_M is the surface exchange coefficient, which consists of a neutral part and a part that is a function of the stability. The boundary condition is calculated with the wind at the second level of the model because the first level is too close to the ground and not of interest to us. For more detail we again refer to Holtslag and Boville (1993). The same equation is used for the v component of the wind, u being replaced by v. The fluxes are evaluated between the vertical grid points, so the tendencies can be calculated from the divergence of the fluxes.

REFERENCES

Arritt, R. W., 1993: Effects of the large scale flow on characteristic features of the sea breeze. *J. Appl. Meteor.*, **32,** 116–125.

Atkinson, B. W., 1981: *Meso-Scale Atmospheric Circulations.* Academic Press, 495 pp.

Banta, R. M., 1995: Sea breezes shallow and deep on the California coast. *Mon. Wea. Rev.*, **123,** 3614–3622.

——, L. D. Olivier, and D. H. Levinson, 1993: Evolution of the Monterey sea-breeze layer as observed by pulsed Doppler lidar. *J. Atmos. Sci.*, **50,** 3959–3982.

Bechtold, P., J.-P. Pinty, and P. Mascart, 1991: A numerical investigation of the influence of large-scale winds on sea-breeze- and land-breeze-type circulations. *J. Appl. Meteor.*, **30,** 1268–1279.

Dalu, G. A., and R. A. Pielke, 1989: An analytical study of the sea breeze. *J. Atmos. Sci.*, **46,** 1815–1825.

Engelbart, D., H. Steinhagen, U. Görsdorf, J. Lippmann, and J. Neisser, 1996: A 1290 MHz profiler with RASS for monitoring wind and temperature in the boundary layer. *Beitr. Phys. Atmos.*, **69,** 63–80.

Estoque, M. A., 1962: The sea breeze as a function of the prevailing synoptic situation. *J. Atmos. Sci.*, **19,** 244–250.

Finkele, K., J. M. Hacker, H. Kraus, and R. A. D. Byron-Scott, 1995: A complete sea-breeze circulation cell derived from aircraft observations. *Bound.-Layer Meteor.*, **25,** 63–88.

Frizzola, J. A., and E. L. Fischer, 1963: A series of sea breeze observations in the New York City area. *J. Appl. Meteor.*, **2,** 722–739.

Holtslag, A. A. M., and B. A. Boville, 1993: Local versus nonlocal boundary-layer diffusion in a global climate model. *J. Climate*, **6,** 1825–1842.

——, E. van Meijgaard, and W. C. de Rooy, 1995: A comparison of boundary layer diffusion schemes in unstable conditions over land. *Bound.-Layer Meteor.*, **66,** 69–95.

Kingsmill, D. E., 1995: Convection initiation associated with a sea-breeze front, a gust front, and their collision. *Mon. Wea. Rev.*, **123,** 2913–2933.

Koo, Y.-S., and D. D. Reible, 1995a: Flow and transport modeling in the sea-breeze. Part I: A modified $E - \epsilon$ model with a non-equilibrium level 2.5 closure. *Bound.-Layer Meteor.*, **75,** 109–140.

——, and ——, 1995b: Flow and transport modeling in the sea-breeze. Part II: Flow model application and pollutant transport. *Bound.-Layer Meteor.*, **75,** 209–234.

Kraus, H., J. M. Hacker, and J. Hartmann, 1990: An observational aircraft-based study of sea-breeze frontogenesis. *Bound.-Layer Meteor.*, **53,** 223–265.

Laird, N. F., D. A. R. Kristovich, R. M. Rauber, H.T. Ochs III, and L. Jay Miller, 1995: The Cape Canaveral sea and river breezes: Kinematic structure and convective initiation. *Mon. Wea. Rev.*, **123,** 2942–2956.

Lu, R., and R. P. Turco, 1994: Air pollutant transport in a coastal environment. Part I: Two-dimensional simulations of sea-breeze and mountain effects. *J. Atmos. Sci.*, **51,** 2285–2308.

Mahrer, Y., and R. A. Pielke, 1977: The effects of topography on sea and land breezes in a two-dimensional numerical model. *Mon. Wea. Rev.*, **105,** 1151–1162.

National Research Council, 1992: *Coastal Meteorology: A Review of the State of the Science*. National Academy Press, 99 pp.

Physick, W. L., 1980: Numerical experiments on the inland penetration of the sea breeze. *Quart. J. Roy. Meteor. Soc.*, **106,** 735–746.

Pielke, R. A., 1974: A three-dimensional numerical model of the sea breezes over South Florida. *Mon. Wea. Rev.*, **102,** 115–139.

Rotunno, R., 1983: On the linear theory of land and sea breeze. *J. Atmos. Sci.*, **40,** 1999–2009.

Schmidt, F. H., 1947: An elementary theory of the land- and sea-breeze circulation. *J. Meteor.*, **4,** 9–15.

Sha, W., T. Kawamura, and H. Ueda, 1993: A numerical study of nocturnal sea breezes: Prefrontal gravity waves in the compensating flow and inland penetration of the sea-breeze cutoff vortex. *J. Atmos. Sci.*, **50,** 1076–1088.

Simpson, J. E., 1994: *Sea Breeze and Local Wind.* Cambridge University Press, 234 pp.

van Ulden, A. P., and A. A. M. Holtslag, 1985: Estimation of atmospheric boundary layer parameters for diffusion applications. *J. Climate Appl. Meteor.*, **24,** 1196–1207.

Xu, Q., M. Xue, and K. K. Droegemeier, 1996: Numerical simulations of density currents in sheared environments within a vertically confined channel. *J. Atmos. Sci.*, **53,** 770–786.